Faraday Discussions

Accepted Manuscript

This manuscript will be presented and discussed at a forthcoming Faraday Discussion meeting. All delegates can contribute to the discussion which will be included in the final volume.

Register now to attend! Full details of all upcoming meetings: http://rsc.li/fd-upcoming-meetings

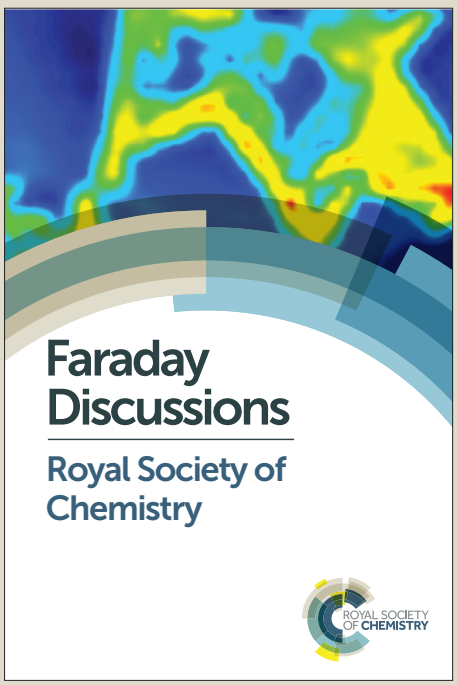

This is an *Accepted Manuscript*, which has been through the Royal Society of Chemistry peer review process and has been accepted for publication.

Accepted Manuscripts are published online shortly after acceptance, before technical editing, formatting and proof reading. Using this free service, authors can make their results available to the community, in citable form, before we publish the edited article. We will replace this *Accepted Manuscript* with the edited and formatted *Advance Article* as soon as it is available.

You can find more information about *Accepted Manuscripts* in the Information for Authors.

Please note that technical editing may introduce minor changes to the text and/or graphics, which may alter content. The journal's standard Terms & Conditions and the Ethical guidelines still apply. In no event shall the Royal Society of Chemistry be held responsible for any errors or omissions in this *Accepted Manuscript* or any consequences arising from the use of any information it contains.

ROYAL SOCIETY OF CHEMISTRY

www.rsc.org/faraday_d

Electrochemistry of $La_{0.3}Sr_{0.7}Fe_{0.7}Cr_{0.3}O_{3-\delta}$ as an Oxygen and Fuel Electrode for RSOFCs

Beatriz Molero-Sánchez, Paul Addo, Aligul Buyukaksoy, Scott Paulson and Viola Birss*

Department of Chemistry, University of Calgary, Calgary, Alberta, Canada T2N 1N4

*To whom correspondence should be addressed. Email: birss@ucalgary.ca

Abstract

The use of a single porous mixed ion-electron conducting (MIEC) material as both the oxygen and fuel electrodes in reversible solid oxide cells is of increasing interest, primarily due to the resulting simplified cell design and lower manufacturing costs. In this work, $La_{0.3}Sr_{0.7}Fe_{0.7}Cr_{0.3}O_{3-\delta}$ (LSFCr-3) was studied in a 3-electrode half-cell configuration in air, pure CO_2 and in a 1:1 CO_2:CO mixture, over a temperature range of 650 – 800 ^oC. A detailed analysis of the impedance (EIS) data, under both open circuit and polarized conditions, as well as the cyclic voltammetry response of LSFCr-3 has shown that it is very active in all of these environments, but with oxygen evolution being somewhat more facile that oxygen reduction, and CO_2 reduction more active than CO oxidation. Evidence for a chemical capacitance, associated with the $Fe^{3+/4+}$ redox process in LSFCr-3, was also obtained from the EIS and CV data in all gas environments.

1. Introduction

As part of the world-wide efforts to identify new energy conversion and storage systems, there is great interest in the development of reversible fuel cells, particularly reversible solid oxide fuel cells (RSOFCs). RSOFCs can run in both the electrolysis mode (SOEC) to store energy by converting H_2O to H_2 and O_2, or co-electrolyze CO_2 and H_2O to syngas and O_2, when excess electricity is available, and then run in the fuel cell mode (SOFC) to convert H_2 or syngas, and oxygen, to electricity and heat when electricity is needed. The primary goal of our recent work has therefore been to develop high performance and stable electrode materials for use in RSOFCs, with our specific focus being on $La_{1-x}Sr_xFe_{1-y}Cr_yO_{3-\delta}$ (LSFCr) and $La_{1-x}Ca_xFe_{1-y}Cr_yO_{3-\delta}$ (LCFCr) mixed ionic-electronic conducting (MIEC) perovskite electrodes, operating at 650-800 ^oC.

In addition to the excellent performance of this family of perovskites as RSOFC electrode materials [1, 2], a key concept behind our work is that these materials can be employed as both the fuel and air electrodes in both the SOFC and SOEC modes, thus significantly lowering cost by decreasing the number of materials used and also by simplifying the manufacturing process. It is worth noting that the latter concept is a relatively new topic of investigation and thus there are only a few studies focussed on developing symmetrical RSOFCs in the literature[1, 3, 4].

Earlier work in our group has shown that the LSFCr perovskite, specifically the Cr-3 member of this family, gives the optimum trade-off between structural, electrical conduction, thermal expansion, and electrochemical properties [1]. LSFCr-3 is a very good air electrode, a promising H_2 electrode [1], and also shows very good promise as a catalyst for CO_2 reduction and CO oxidation[5]. However, a detailed analysis of the electrochemistry of these reactions at this material has not yet been carried out. Our preliminary work showed that LSFCr-3 and LCFCr-3

are both promising as RSOFC electrodes, although LCFCr-3 has the better thermal expansion compatibility with YSZ (yttria-stabilized zirconia) [2]. Even so, the focus in the present work is on LSFCr-3, as a broader set of results are available for this MIEC material.

In this paper, the electrochemical performance of LSFCr-3 has been studied in detail, both at open circuit and under polarization, at between 650 and 800 ^{o}C in air, pure CO_2 and CO_2/CO mixtures. Importantly, all of this work has involved a 3-electrode configuration. Notably, in-depth studies of the performance and stability of oxygen and fuel electrodes using a 3 electrode setup, especially under polarization, are lacking in the literature, making it difficult to deduce reaction mechanisms. It is shown here that the performance of this material in all of the gas environments is very good, although CO oxidation is the most inhibited. Efforts are also made to understand the slow steps in these reactions, based primarily on the interpretation of the electrochemical impedance spectroscopy and cyclic voltammetry data collected for the LSFCr-3 electrode.

2. Experimental Methods

2.1 Electrode material preparation

$La_{0.3}Sr_{0.7}Fe_{0.7}Cr_{0.3}O_{3-\delta}$ (LCFCr-3) powders were prepared by the combustion method starting with nitrate precursors. Details of the synthetic procedure have been published elsewhere[1].

2.2 Half-cell construction

The $La_{0.3}Sr_{0.7}Fe_{0.7}Cr_{0.3}O_{3-\delta}$ powders, obtained from the regular combustion method [1], were milled (high energy planetary ball mill, Pulverisette 5, Fritsch, Germany) in an isopropanol

medium at a rotation speed of 300 rpm for 2 h using zirconia balls. A $Gd_{0.9}Ce_{0.1}O_{2-\delta}$ (GDC) buffer layer for the working, counter and reference electrodes was screen printed onto both sides of a 300 μm thick, dense YSZ electrolyte (Fuel Cell Materials), followed by firing at 1200 ºC for 2 hours. The ca. 30 μm thick LSFCr-3 working (WE) and counter (CE) electrodes were then screen-printed symmetrically (over an area of 0.5 cm^2) onto both sides of the GDC buffer layer. LSFCr-3 was also used as the reference electrode (RE), screen-printed onto the same side of the YSZ, as the working electrode (WE), placed 2 to 4 mm from the WE to prevent electrode geometry artifacts. The LSFCr-3 electrodes were then fired at 1100 ºC for 2 h. Au paste (C 5729, Heraeus Inc., Germany) was painted on all three electrode layers to serve as the current collectors.

2.3 Electrochemical studies

In all of this work, the electrochemical measurements to evaluate the cell performance were performed using 3 electrode methods in a range of gas atmospheres (pO_2 = 1-10^{-18}), with a total flow rate of 50 ml/min, and a range of temperatures. Electrochemical Impedance spectra (EIS) were collected under open circuit and polarized conditions between 650 ºC and 800 ºC, using an amplitude of 50 mV in the frequency range of 0.01 to 65 kHz and using a Solartron 1287/1255 potentiostat/galvanostat/impedance analyzer. Zview software was used to fit and analyze the impedance data. CV measurements (sweep rates from 1-10 mV/s) between -0.7 V and 0.7 V vs. the RE were performed using a Solartron 1287 interface, with control and data collection handled by Corrware software.

3. Results and Discussion

3.1 Oxygen reduction and evolution at LSFCr-3

The electrochemical activity towards both the oxygen reduction (ORR) and evolution (OER) reactions was examined by cyclic voltammetry (CV) and electrochemical impedance spectroscopy (EIS) at pO_2 = 0.1-1 atm and 650-800 ^oC. The EIS data were collected both at the open circuit potential (OCP) when the oxygen reaction is at equilibrium, and also under polarization (± 0.3 V), conditions under which either the ORR or OER is the dominant reaction. While this approach is not commonly used in the literature in SOFC/SOEC studies, and especially not for mixed ion and electron conducting (MIEC) oxide electrodes, there have been a few efforts made in this direction, including determining the effect of polarization on the electrochemical behavior of La_2NiO_4, LSM, LSF and LSCF [6-9].

3.1.1 Open Circuit EIS Studies

3-electrode AC impedance measurements were carried out initially at the open circuit potential (OCP) in air using the LSFCr-3/GDC/YSZ/GDC/LSFCr-3 cells, with LSFCr-3 also used as the reference electrode. Fig. 1a shows the typical impedance spectra obtained for LSFCr-3 at open circuit under an oxygen partial pressure of 0.21 atm at temperatures between 650 and 800 ^oC. Some high frequency noise and an inductance were sometimes observed during these measurements, generally attributed to the instrument and the leads, and thus ignored. In all cases, two time constants were clearly observed over the full temperature range at the OCP, revealing two different processes in the oxygen reaction at LSFCr-3. Thus, all of the spectra obtained in oxygen atmospheres were fitted using the equivalent circuit RS(R2/CPE)(R3/CPE) shown in Fig. 1b, with the best-fit values of the circuit elements given in Table 1. RS

corresponds to the series resistance, arising from the contacts, leads and the resistance of the electrolyte between the WE and RE, while the sum of R2 (high frequency, (RHF)) and R3 (low frequency, (RLF)) is equivalent to the total polarization resistance (Rp).

The CPEs are constant phase elements and were converted to capacitors using the following equation (1) [10]:

$$C_i = (R_i Q_i)^{1/ni} / R_i \quad (1)$$

where R is a resistance and Q is a constant phase element (CPE), representing time-dependent capacitive elements, and n is the associated parameter which indicates the similarity of Q to an ideal capacitor, for which n = 1.

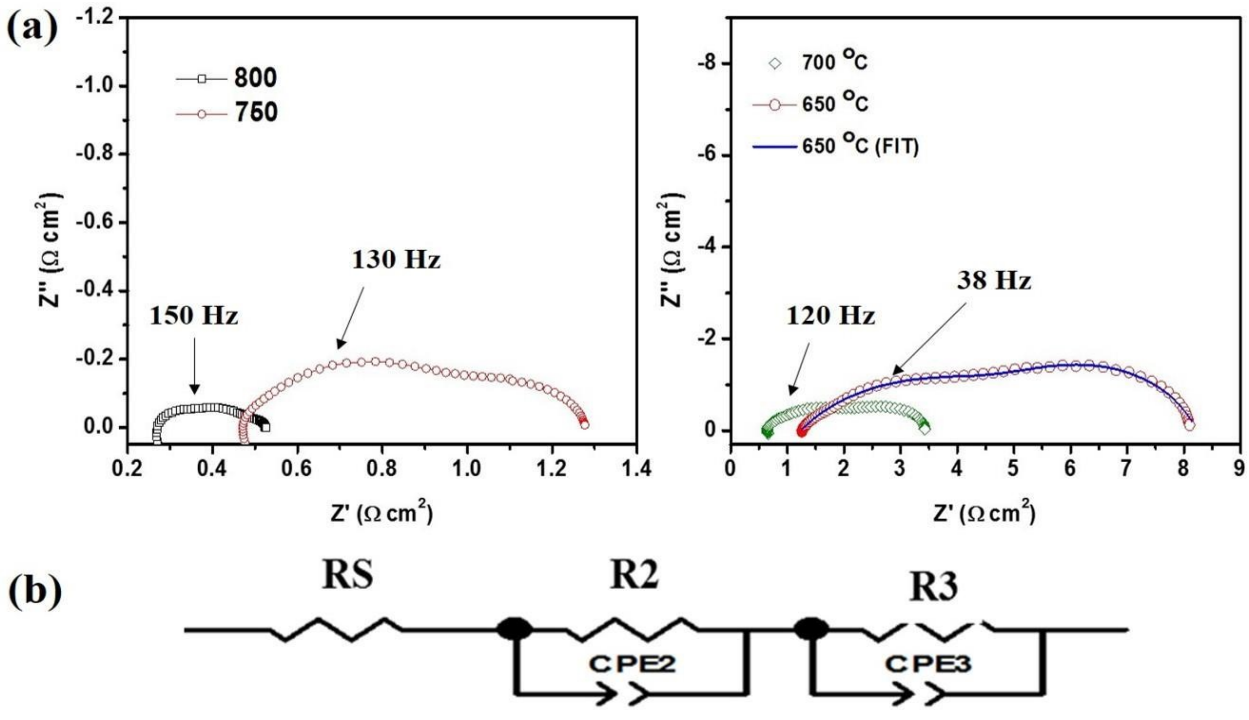

Fig. 1 (a) Typical impedance spectra of a LSFCr-3 working electrode in a 3-electrode half-cell configuration at open circuit under an oxygen partial pressure of 0.21 atm and variable temperatures. (b) Equivalent circuit used for data fitting.

Table 1. Circuit elements* associated with the data in Fig. 1**

T (ºC)	RHF (Ω.cm^2)	RLF (Ω.cm^2)	CHF (F/cm^2)	CLF (F/cm^2)	n HF	n LF
800	0.26	0.02	$1.5x10^{-3}$	$2x10^{-1}$	0.64	0.70
750	0.53	0.27	$2.3x10^{-3}$	$2.0x10^{-1}$	0.71	0.79
700	1.9	1.02	$1.8x10^{-3}$	$1.8x10^{-1}$	0.77	0.55
650	4.1	2.9	$2.8x10^{-3}$	$1.6x10^{-1}$	0.81	0.58

*(RHF, CHF, nHF) are obtained from the high frequency arc, while (RLF,CLF,nLF) are from the low frequency arc.
** Three electrode LSFCr-3 half-cell configuration, pO_2 = 0.21 atm, 50 ml/min flow rate.

Table 1 shows that the resistance associated with the process at high frequencies (RHF), often ascribed to the charge transfer reaction, increases with decreasing temperature, from 0.26 to 4.1 Ω cm^2, as expected for this type of process, while the associated capacitance (CHF) remains almost unchanged at ca. $2x10^{-3}$ F cm^{-2} (Table 1). The resistance of the low frequency arc (RLF) at the OCP (Table 1) decreases even more noticeably with increasing temperature (Table 1) and thus cannot be related to gas phase diffusion limitations, which are known to be almost temperature independent[10]. Its associated capacitance (CLF) is very large, typical of the chemical capacitance obtained when using MIEC electrodes[1, 11] and related to their redox chemistry.

A series of experiments involving varying pO_2 (0.1-1 atm) was then conducted to elucidate the effect of the oxygen partial pressure on the EIS response at equilibrium (at the OCP). Fig. 2 shows a set of open circuit EIS data at 700 ºC, as an example, and Table 2 shows the resistance and capacitance values for the high (HF) and low frequencies (LF) processes, obtained by fitting

the Fig. 2 data to the same equivalent circuit as shown in Fig. 1b and using equation (1) to convert the CPEs to capacitance values. Rs and RHF are seen to be independent of pO_2, as expected, (Table 2) and CHF remains almost unchanged at ca. $1.8x10^{-3}$ F cm^{-2} (Table 2).

In contrast, the resistance associated with the low frequency arc decreases quite significantly with increasing pO_2, while CLF hardly changes, but remains large, typical of a chemical capacitance. As shown in Fig. 2a, the low frequency arc is absent in pure oxygen (pO_2 = 1). However, when pO_2 was decreased to 0.2 atm, the low frequency arc is easily discerned in both the Bode and Nyquist depictions, centered at ca. 3.6 Hz (Fig. 2b). Thus, the process associated with the low frequency arc is strongly affected by oxygen only when pO_2 is low (below 0.2 atm). As this arc is not diffusional (gas phase) in nature, this may point to surface reactions involving oxygen (e.g., oxygen adsorption or dissociation) as the slow step. Similar characteristics have been reported by several authors for the ORR/OER at the OCP at La_{1-x} Sr_xMnO_3 (LSM), $La_{0.6}Sr_{0.4}Co_{0.2}Fe_{0.8}O_{3-\delta}$ (LSCF) and La_2NiO_4 electrodes[10, 12-16].

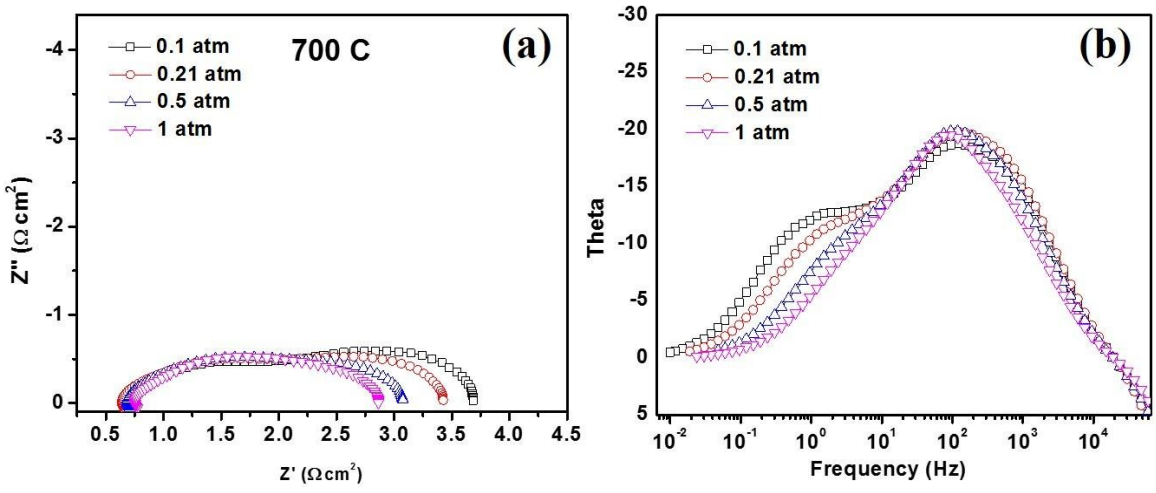

Fig. 2 (a) Nyquist and (b) Bode phase angle plots of a LSFCr-3 working electrode in a 3-electrode half-cell configuration, evaluated at a pO_2 of 0.1, 0.21, 0.5 and 1 atm, all at 700 ^oC.

Table 2. Circuit elements* associated with the impedance data in Fig. 2**

pO_2 (atm)	RHF ($\Omega.cm^2$)	RLF ($\Omega.cm^2$)	CHF# (F/cm^2)	CLF# (F/cm^2)	n HF	n LF
0.1	1.63	1.61	$1.5x10^{-3}$	$1.6x10^{-1}$	0.59	0.73
0.21	1.96	1.02	$1.8x10^{-3}$	$1.9x10^{-1}$	0.54	0.78
0.5	2.04	0.56	$1.9x10^{-3}$	$2.0x10^{-1}$	0.56	0.86
1	2.08	0.22	$2.3x10^{-3}$	$3.4x10^{-1}$	0.58	1.0

*(RHF, CHF, nHF) are obtained from the high frequency arc, while (RLF,CLF,nLF) are from the low frequency arc.
** Three electrode LSFCr-3 half-cell configuration, 700 ^oC, 50 ml/min flow rate.
# CHF and CLF represent the high and low frequency arcs, respectively, and were obtained by fitting to the equivalent circuit shown in Fig. 1b, and calculated by using $C = (R*CPE)^{1/n}/R$ [10].

The ORR (and the reverse OER) are known to be very complex, occurring in multiple elementary steps, with one mechanism suggested to be [17]: (1) diffusion of O_2 molecules from the gas phase to the active site, (2) oxygen dissociative adsorption on the cathode surface, (3) electron transfer step, (4) incorporation of O^{2-} into the electrode at the double phase boundary (DPB), (5) O^{2-} diffusion in the bulk of cathode, and (6) O^{2-} transfer from the cathode to electrolyte [17]. Any one of these steps can be rate-determining (the rds), and if microscopic reversibility applies, this step should also be slow during the OER. Using conventional electrochemical theory (Butler-Volmer[18]) and depending on which step is the slowest, a different Tafel slope and hence transfer coefficient (α value, inversely proportional to the Tafel slope[19]) should be obtained. Another parameter that helps in determining the rds of electrochemical reactions is the reaction order (m), in this case with respect to oxygen. For studies done at the

OCP, m can be obtained from the dependence of Rp on the oxygen partial pressure, following equation (2) [17]:

$$Rp^{-1} \propto P_{O_2}^{m} \quad (2)$$

Considering the mechanism above and assuming that the rate of each individual step is 10 times or more different from the previous or following steps so that they can be distinguished kinetically from each other, then for m = 1, molecular oxygen should be involved in the rate-determining step, when m = 1/2, atomic oxygen is involved in the rate-determining step, and when m = 1/4, then charge transfer is the rate-determining process [17].

3.1.2 Polarized EIS Studies

To further investigate the performance of LSFCr-3 towards both the ORR and OER, polarized EIS analysis was carried out in air, with the application of an overpotential of 300 mV in both the positive (SOEC) and negative (SOFC) directions. OCP and polarized Nyquist (Fig. 3a) and Bode (Fig. 3b) plots are shown at a pO_2 of 0.21 atm and 700 ºC under these conditions, as an example. Under polarization, a decrease in the polarization resistance is seen from 2.98 Ω cm^2 at the OCP to 1.63 Ω cm^2 at -300 mV (ORR), while it is 1.03 Ω cm^2 at +300 mV (OER), as expected.

In general terms, under positive polarization, a somewhat less suppressed low frequency arc is observed than under negative polarization (Fig. 3a), consistent with what is seen in the Bode plots (Fig. 3b). Moreover, the arcs under either OCP or negative polarization remain at the same frequency, while under positive polarization, both arcs shift to higher frequencies and the high frequency resistance diminishes greatly. These results show that there are some important differences between the ORR and the OER that could not have been detected at the OCP, but do

need to be better understood. In relation to this, when anodically polarized EIS was performed in variable pO_2 atmospheres, i.e., under active OER conditions (data not shown), Rp is independent of pO_2 from 0.1 atm to 1 atm. This suggests that the local pO_2 must be dominated by the oxygen generated electrochemically, rather than by the pO_2 of the gas stream passed through the cell. This phenomenon is also seen in the CV data, as will be shown below.

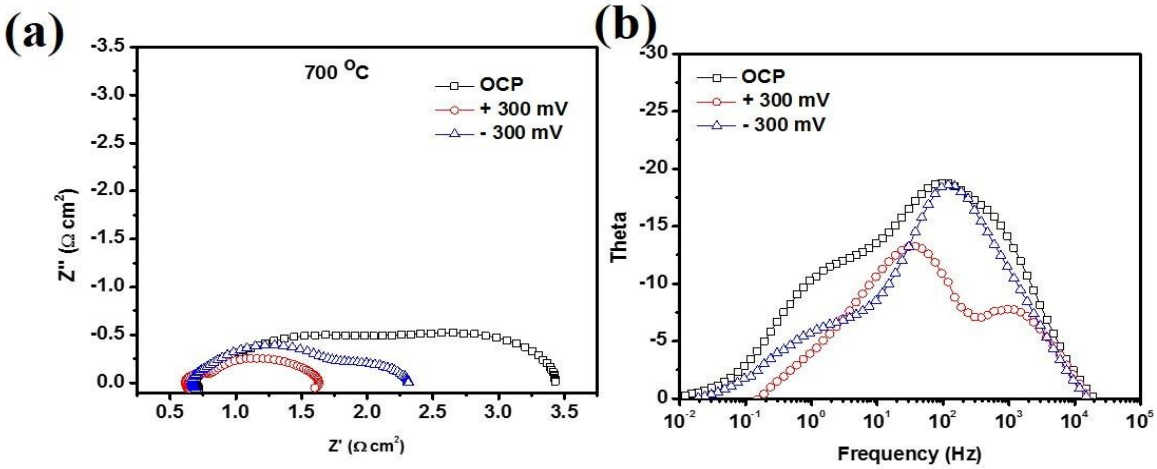

Fig. 3 (a) Nyquist and (b) phase angle Bode plots of the OCP and polarized impedance data of a LSFCr-3 working electrode in a 3-electrode half-cell configuration, evaluated under an oxygen partial pressure of 0.21 atm at 700 °C.

Table 3. Circuit elements obtained by fitting of impedance data* in Figure 3**

Potential of WE	RHF ($\Omega.cm^2$)	RLF ($\Omega.cm^2$)	CHF# (F/cm^2)	CLF# (F/cm^2)	nHF	nLF
OCP	1.96	1.02	$1.8x\ 10^{-3}$	$1.9x10^{-1}$	0.55	0.78
+ 300 mV (OER)	0.12	0.91	$5x10^{-4}$	$1.1x10^{-2}$	1.00	0.73
- 300 mV (ORR)	0.91	0.72	$4.2x10^{-3}$	$1.2x10^{-2}$	0.89	0.44

*(RHF, CHF, nHF) are obtained from the high frequency arc, while (RLF, CLF, nLF) are from the low frequency arc, with the data fitted to the circuit shown in Fig. 1b.
** Three electrode LSFCr-3 half-cell configuration, 700 °C, 0.21 atm pO_2, 50 ml/min flow rate.
# CHF and CLF represent the high and low frequency arcs, respectively, and were calculated by using $C = (R*CPE)^{1/n}/R$ [10].

As expected, the resistance of the high frequency arc decreases under polarization (Table 3), especially at +300 mV, while the associated CHF value increases as the potential is changed from + 300 to -300 mV. Thus the time constant changes quite significantly for the HF arc. In terms of RLF, this circuit element decreases slightly with polarization, which may again suggest that RLF is related to molecular oxygen dissociation/adsorption/desorption processes[15, 16]. Further, the capacitance associated with the low frequency process changes equally with anodic and cathodic polarization, becoming ca. 10^{-2} F cm^{-2} in both cases (Table 3).

In order to better understand the OER and ORR at the LSFCr-3 materials, pO_2 dependence studies were also carried out under polarization to obtain the reaction orders in comparison with those at the OCP. This is not normally done in the literature, but is actually quite important, especially as it is not clear whether the OCP EIS data correctly predicts oxygen electrochemistry at MIEC electrodes under relevant polarization conditions. Fig. 4 displays the dependence of the total polarization resistance (ASRp) on the oxygen partial pressure at 650, 700, 750 and 800 ^{o}C at both the OCP, and at +300 and -300 mV vs. the OCP, with the m values given in Table 4.

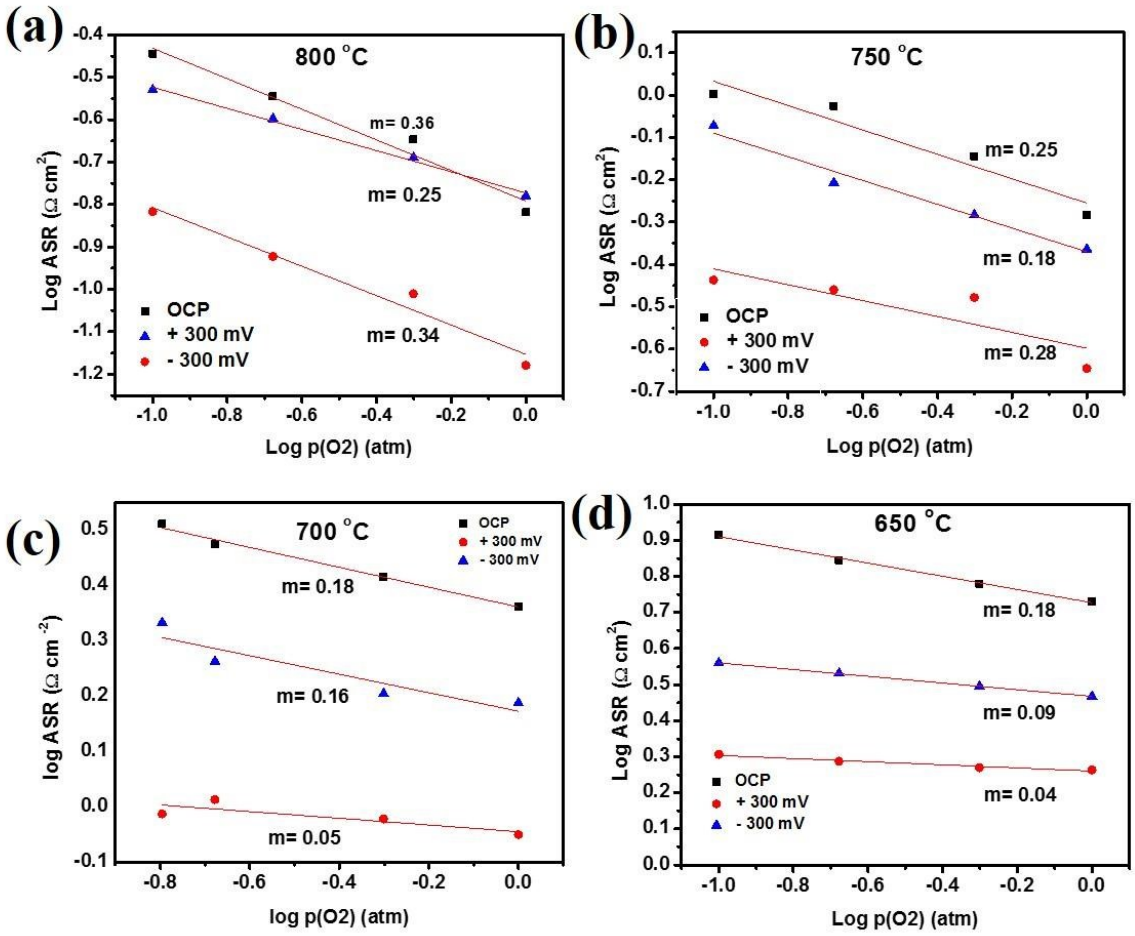

Fig. 4 $p(O_2)$ dependence of ASRp of the LSFCr-3 WE at the OCP and at both anodic (300 mV) and cathodic (-300 mV) overpotentials at (a) 800 °C, (b) 750 °C, (c) 700 °C, and (d) 650 °C, also showing the corresponding *m* values at different temperatures.

Table 4. Reaction order *(m)* with respect to O_2 at various potentials and temperatures (from Fig. 4)*

Temperature (°C) / Potential (mV)	800	750	700	650
OCP	0.36	0.25	0.18	0.18
+ 300	0.25	0.18	0.05	0.04
- 300	0.35	0.28	0.16	0.09

* Three electrode (LSFCr-3) half-cell configuration, 50 ml/min flow rate.

From Table 4, it is seen that the reaction orders, obtained from Rp at the OCP and at negative overpotentials, are similarly pO_2 dependant at all temperatures. Furthermore, the reaction orders at positive overpotentials (OER) seem to be less dependent on pO_2 than those at the OCP and under negative polarization, as fully expected, as oxygen is the product of the OER.

To further investigate the pO_2 dependence of the high and low frequency processes, the pO_2 dependence of each of the resistances identified from the EIS studies at both the OCP and at polarization is shown in Fig. 5, for the example of 700 °C. A very strong pO_2 dependence (m = 0.99) of the low frequency process at OCP conditions is observed in Table 5, which suggests that molecular oxygen involved in the slowest step at the OCP, either adsorbing to the surface, or dissociating. This observation clearly supports our previous discussion about the low frequency process.

On the other hand, the high frequency process shows only a weak oxygen partial pressure dependence (m = 0.1) at the OCP. According to past studies[10, 15], this may indicate that a charge transfer step is the rate determining process. Moreover, the pO_2 dependence of both high and low frequency processes under positive and negative polarization, shown in Table 5, indicates a very

weak pO_2 dependence for both the ORR and OER reactions, and very different dependencies with respect to what is seen at the OCP. These data confirm the earlier conclusions, namely that during the OER, the O_2 that is being produced generates a local pO_2 makes that makes the rate of the reaction independent of the external pO_2. On the other hand, in the negative direction (ORR), we observe no pO_2 dependence for the high frequency feature, but a slightly stronger dependence at low frequencies.

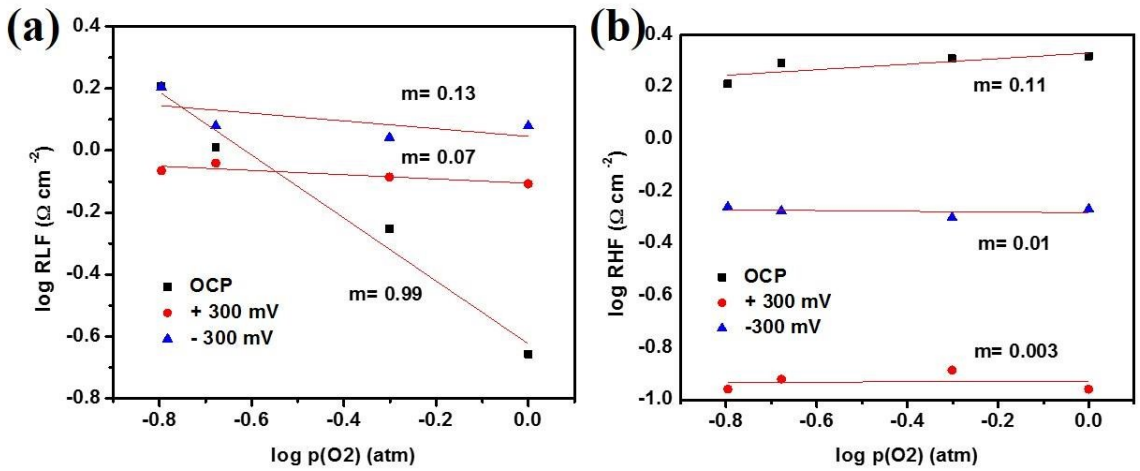

Fig. 5 pO_2 dependence of the (a) low and (b) high frequency processes observed at LCFCr-3 WE at the OCP and at anodic and cathodic overpotentials at 700 ^oC.

Table 5. Reaction order (*m*) of O_2 at 700 ^oC at the OCP and under positive and negative polarization*

Potential (mV)	*m* (low frequencies)	*m* (high Frequencies)
OCP	0.99	0.11
+ 300	0.07	0.003
- 300	0.13	0.01

* Three electrode (LSFCr-3) half-cell configuration, 50 ml/min flow rate, based on data in Fig. 5.

3.1.3 Cyclic Voltammetry Studies

The cyclic voltammetry (CV) response of the ORR and OER at the LSFCr-3 electrodes was also investigated, revealing that it was independent of potential sweep rate and gas flow rate. This indicates there are no bulk mass transport limitations associated with getting O_2 to or from the electrode surface. Fig. 6a shows the effect of pO_2 at constant temperature (800 ^oC), while Fig. 6b shows the effect of temperature on the CV behavior a constant oxygen partial pressure of 0.21 atm.

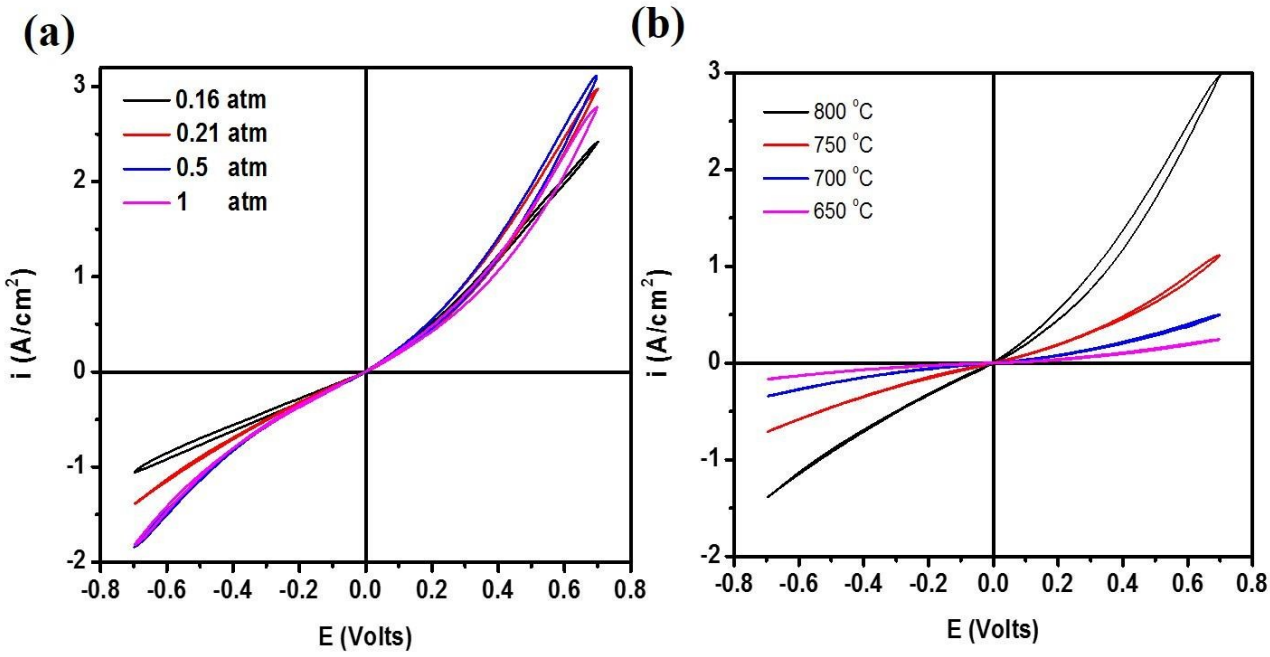

Fig. 6 Cyclic voltammograms (5 mV/s) for LSFCr-3 WE in 3 electrode half-cell configuration evaluated (a) at various p (O_2) at 800 ^oC and (b) at various temperatures at 0.21 atm pO_2.

It is worth noting that LSFCr-3 appears to be a significantly better catalyst for the OER reaction as opposed to the ORR, as seen in the asymmetrical nature of all of the CVs, similar to the Ca analogue, LCFCr-3 [20]. This is consistent with the polarized EIS data in Table 3, where Rp is 1.03 Ω cm^2 at +300 mV and 1.63 Ω cm^2 at -300 mV. As expected, the currents increase with increasing pO_2 in the ORR region, except at 1 atm (Fig. 6a), consistent with the effect of O_2 on

the EIS results (Fig. 2). However, in the OER region, no obvious effect is observed when the pO_2 is increased from 0.16 to 1 atm, as O_2 is the reaction product in the OER and should thus not affect its kinetics under anodic polarization. On the other hand, the effect of temperature on the OER and ORR is very pronounced, as shown in Fig. 6b, confirming again that the slow step in either of these reaction is not mass transport in the gas phase.

A key kinetic parameter obtained from CV analysis is i_o, the exchange current density. The i_o values, obtained using low-field analysis (equation 3)[19, 21] of the CV data (Fig. 6b) are shown in Table 6 and were also compared to those obtained from Rp in the OCP EIS data (Fig. 1).

$$i_o = (RT\nu/nF)\ \text{slope} \qquad (3)$$

where the slope is obtained from the i-V plots (Fig. 6b) within ± 50 mV of the OCP, and assuming that n = 4 and v = 1, where n is the total number of electrons transferred in the oxygen reaction (i.e., 4) and v is the stoichiometric coefficient (ORR mechanisms proposed in the literature suggest a value of 1 [21]).

The exchange current density values (Table 6) show relatively good agreement for the results obtained using these two electrochemical techniques. Overall, this adds confidence that the open circuit and polarized 3-electrode experiments, and the associated data analysis methods used, have been carried out correctly in this work.

Table 6. Exchange current densities (i_o) obtained by CV* and EIS measurements (Figs. 1 and 6b)**

Temperature (°C)	CV i_o (A cm $^{-2}$)	EIS i_o (A cm $^{-2}$)
800	0.12	0.09
750	0.026	0.02
700	0.015	0.007
650	0.005	0.004

* Fitted parameters are based on the low field approximation in the potential range of ± 50 mV vs. the OCP in Fig. 6b.
** Based on Rp obtained from EIS experiments (Table 1).

3.2 Three electrode CO_2 reduction and CO oxidation studies

The electrochemical performance and stability of the LSFCr-3 material towards the reduction of CO_2 and oxidation of CO was also investigated here. A 3 electrode half-cell was again constructed, with LSFCr-3 pasted on both sides of the YSZ electrolyte, a LSFCr reference electrode attached on the WE side, and a GDC buffer layer present between YSZ and the LSFCr-3 electrodes.

3.2.1 100% CO_2 Studies

Fig. 7 shows both the open circuit and polarized impedance data (all at an overpotential of ± 100 mV), obtained for LSFCr-3 in a pure CO_2 atmosphere, showing three well-defined time constants, with one process seen at high frequencies (R1/CPE1) and two at low frequencies (R2/CPE2 and R3/CPE3). CO_2 alone was investigated in an attempt to simplify data interpretation and help to identify any diffusion controlled processes, as CO will be present in very low concentrations under these conditions, generated only as the product of CO_2 reduction.

As expected, the full polarization resistance (Rp = R1+R2+R3) is smaller at negative polarization during CO_2 reduction than at the OCP, and is the largest at +100 mV polarization in the absence of CO in the gas feed stream. To further understand the various processes occurring in this cell, the EIS data, obtained both at the OCP and under polarization, were fitted to the Rs(R1/CPE1)(R2/CPE2)(R3/CPE3) equivalent circuit, where the CPEs were again converted to capacitance (C) using equation (1). Table 7 shows the values of the circuit elements and the calculated capacitances under all of these conditions.

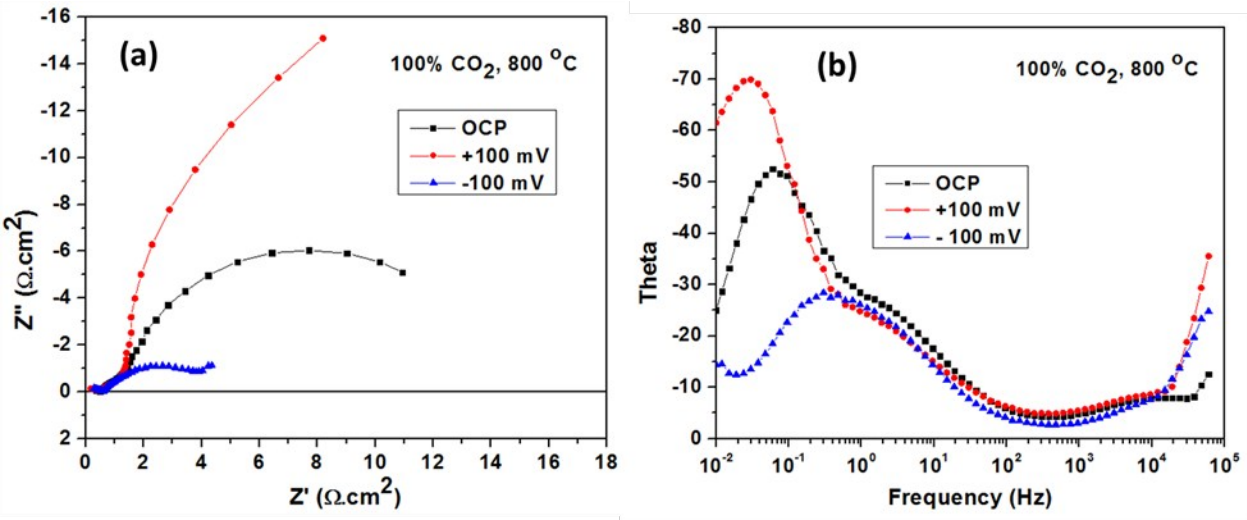

Fig. 7 OCP and polarized (± 100 mV) EIS response of LSFCr-3 in three electrode half-cell, operated at 800 ºC in 100% CO_2, showing (a) the Nyquist plots and (b) the phase angle Bode plots.

Table 7. Fitted parameters* from Figure 7a using the Rs(R1/CPE1)(R2/CPE2)(R3/CPE3) equivalent circuit model**

Potential (mV)	R1 ($\Omega.cm^2$)	C1# (F/cm^2)	n1	R2 ($\Omega.cm^2$)	C2# (F/cm^2)	n2	R3 ($\Omega.cm^2$)	C3# (F/cm^2)	n3	Rp ($\Omega.cm^2$)
OCP	0.20	$8.66x10^{-5}$	0.64	1.09	0.131	0.67	12.6	0.68	0.97	13.9
+100	0.45	$6.53x10^{-6}$	0.38	0.91	0.143	0.71	40.7	0.85	1.00	42.1
-100	0.22	$8.19x10^{-5}$	0.64	0.87	0.172	0.67	2.77	0.67	0.82	3.85

*(R1, C1, n1) were obtained from the high frequency (10 kHz) arc, while (R2, C2, n2) and (R3, C3, n3) are from the low (1 Hz) and still lower (0.05 Hz) frequency arcs, respectively.
**Three electrode LSFCr-3 half-cell, operated at 800 ^oC in 100% CO_2.
C1, C2 and C3 represent the high, low and lower frequency arcs, respectively, and were calculated using equation (1).

The resistance associated with the high frequency arc (R1) is suggested to be due to a charge transfer process. This interpretation is strengthened by the relatively low value of the parallel capacitor (C1), 0.6 - 0.9 x 10^{-5} F/cm^2, which is typical for an interfacial capacitance. The weak dependence of R1 on overpotential is consistent with being in the 'low field' region, i.e., at ± 100 mV polarization, and thus R1 would be expected to be very similar to the value obtained at the OCP. The low frequency arc (R3/C3) is ascribed to a gas diffusion process, as the C3 values are very large, in the range of 0.67- 0.85 F/cm^2, and are essentially independent of overpotential. Also, the n3 values are generally close to unity. R3 is much higher under anodic vs. cathodic polarization, presumably because there is no CO in the gas stream and thus only the small quantities of CO generated during CO_2 reduction are available for the oxidation process under anodic polarization. In contrast, under cathodic polarization, R3 is quite small, since CO_2 is being rapidly reduced to CO.

The meaning of R2 and C2 is less clear. C2 may be reflective of the chemical capacitance (changes in stiochiometry) of the LSFCr material, similar to the interpretation used in the air

study above. As seen in Table 7, C2 is in the range of 0.13-0.17 F/cm^2, observed at ca. 1 Hz, and is relatively independent of polarization. The fact that C2 is the largest at -100 mV (0.17 F/cm^2), vs. at the OCP and at +100 mV polarization, may indicate that more oxygen vacancies are created in this potential range due to the enhanced redox chemistry of Fe^{4+} to Fe^{3+} in LSFCr-3 under these conditions. R2 is only very weakly dependent on overpotential and thus it is possible that it reflects an interfacial process, such as oxygen ion vacancy formation/filling in the LSFCr-3 lattice, which probably influences the CO_2/CO adsorption/dissociation step.

Cyclic voltammetry (CV) was also carried out to obtain further insights into the electrochemical mechanism of CO_2 reduction and CO oxidation at the LSFCr-3 electrode. Fig. 8 shows the 3-electrode CV in pure CO_2 at 800 ^oC at 5 mV/s. The CV shows higher current densities in the cathodic scan than in the anodic direction, which is not surprising, since there is no CO in the gas stream. This is confirmed by the anodic limiting current density behavior (concentration polarization) observed from 0 to + 0.7 V, in full agreement with the EIS data and the discussion of Fig. 7.

In the cathodic direction, Fig. 8 shows a gradually increasing current density as CO_2 reduction commences, with a peak observed at ca. -0.25 V. A similar peak has been reported by Sapountzi et al [22], using $La_{0.75}Sr_{0.25}Cr_{0.9}Fe_{0.1}O_3$ in CO/CO_2 atmospheres, and has been attributed to the redox chemistry of the perovskite oxide. Here, it is proposed that this peak reflects the reduction of Fe^{4+} to Fe^{3+} in the LSFCr-3 lattice, or at least on the oxide surface, with the associated formation of oxide ion vacancies, equivalent to the chemical capacitance seen in the EIS results in Fig. 7. It is uncertain, however, why a matching anodic peak is not observed in the positive scan, regenerating the Fe^{4+} content.

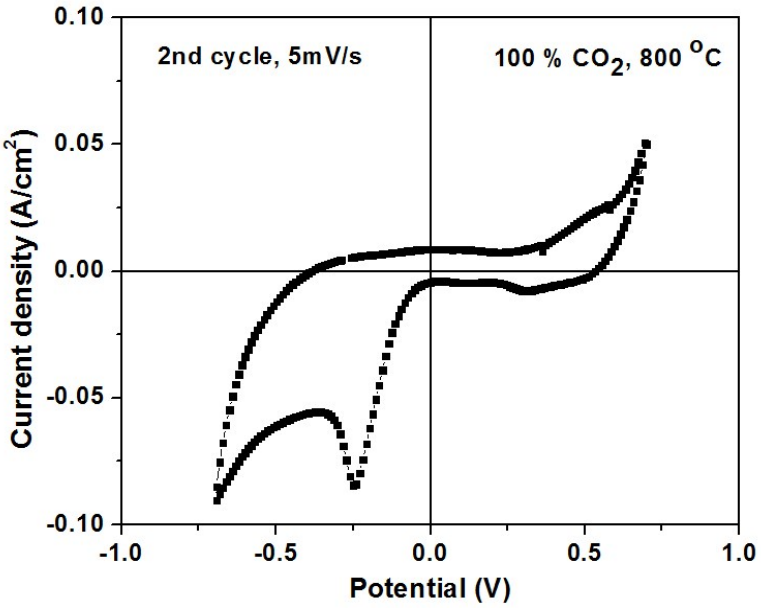

Fig. 8 Cyclic voltammetry data obtained for LSFCr-3 WE in three electrode half-cell, operated at 800 ^{o}C in pure CO_2 at 5 mV/s.

3.2.2 50:50 CO_2:CO Studies

To further evaluate the performance of the LSFCr-3 catalyst towards CO_2 reduction and also CO oxidation, a CO_2:CO ratio of 1:1 was fed to the cell. Fig. 9 shows the OCP and polarized EIS data at 800 ^{o}C in 30% CO_2:30% CO:40% N_2. The impedance data show again that the cell performs better in the cathodic mode (reduction of CO_2) than in the anodic mode (CO oxidation), suggesting that there are some real kinetic differences between these two reactions.

The EIS data were fitted to a Rs(R1/CPE1)(R2/CPE2) equivalent circuit model, with only two time constants appearing under these CO_2/CO conditions (Fig. 9). The (R3/CPE3) time constant, observed at very low frequencies (0.05 Hz) in the pure CO_2 environment in Fig. 7a and ascribed to gas phase diffusion limitations, is minimal or barely detectable in Fig. 9a and thus it was excluded from the fitting model. Table 8 shows the fitted parameters, demonstrating that the polarization resistance at the OCP is 0.87 Ω cm^2, while at +100 mV, it is 1.35 Ω cm^2, and at -100 mV, Rp is 0.67 Ω cm^2.

In the CO_2/CO system (Fig. 9), the low frequency C2 element (Table 8) is now slightly higher in value than in % 100 CO_2 (Table 7). If it is still ascribed to the LSFCr-3 chemical capacitance, then this is perhaps not surprising because the cell is now in a more reducing environment, which would lead to an increase in the concentration of oxygen vacancies as more of the B site cations are reduced. The n2 parameter in the CO_2/CO atmosphere remains unchanged vs. the situation in pure CO_2 (Table 7), showing values of around 0.65, independent of potential. However, R2 in the CO_2/CO atmosphere, assigned in the pure CO_2 studies to be due to an interfacial process, such as oxygen ion vacancy formation/filling in LSFCr-3, possibly affecting the CO_2/CO adsorption and dissociation process, is about 50% lower than in pure CO_2 at both the OCP and at -100 mV, while R2 in the CO_2/CO environment at +100 mV is the same as in pure CO_2.

Again, the high frequency resistance (R1) in the CO_2/CO environment is ascribed to the charge transfer process, as was also the case in the 100% CO_2 and air studies. Also, the high frequency C1 values are typical of interfacial capacitances (10^{-5} F/cm^2), as was also the case in 100% CO_2 and in the air studies.

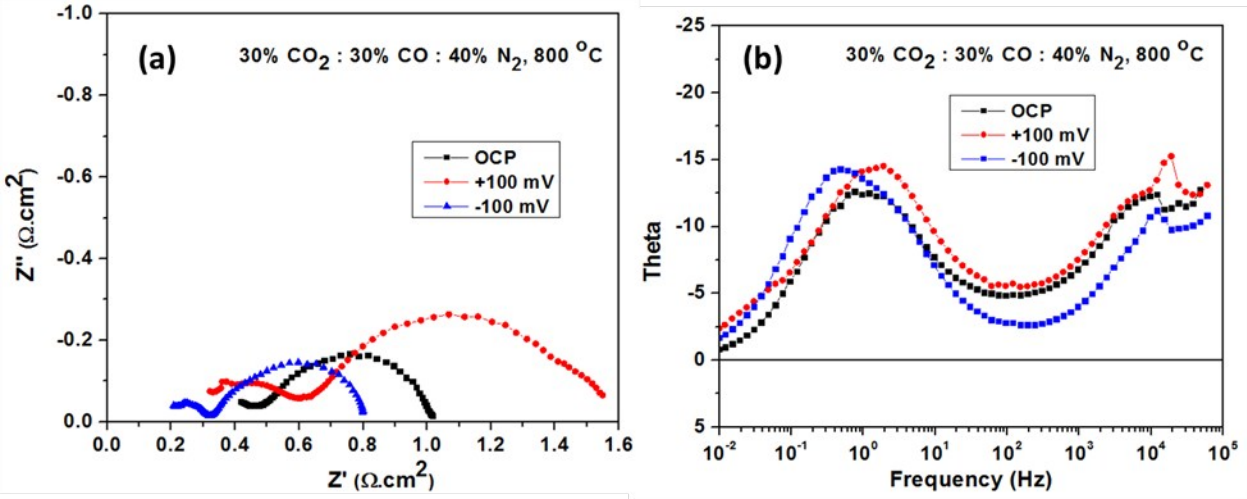

Fig. 9 OCP and polarized (± 0.1 V) EIS response of the LSFCr-3 WE in 3 electrode half cell experiment at 800 °C in 30% CO_2:30%CO:40% N_2, showing (a) the Nyquist plots and (b) the phase angle Bode plots.

Table 8. Fitted parameters* from Figure 9a using the Rs(R1/CPE1)(R2/CPE2) equivalent circuit model.**

Potential (mV)	R1 (Ω.cm^2)	C1$^{\#}$ (F/cm^2)	n1	R2 (Ω.cm^2)	C2$^{\#}$ (F/cm^2)	n2	Rp (Ω.cm^2)
OCP	0.31	5.75x10^{-5}	0.52	0.57	0.47	0.65	0.87
+100	0.41	4.78x10^{-5}	0.53	0.94	0.26	0.63	1.35
-100	0.16	9.12x10^{-5}	0.65	0.51	0.86	0.66	0.67

*(R1, C1, n1) and (R2, C2, n2) obtained from the high (10 kHz) and low (1 Hz) frequency arcs, respectively.
** Three electrode (LSFCr-3) half-cell, operated at 800 °C in 30% CO_2:30%CO:40% N_2.
# C1 and C2 represent the capacitance in the high and low frequencies arcs, respectively and were calculated using equation (1).

Fig. 10 shows the CV of the LSFCr-3 WE in 30% CO_2:30% CO:40% N_2 at 1 mV/s at 800 °C. It is interesting to note that much higher current densities are observed in the negative scan during the reduction of CO_2 to CO than in the positive scan during the oxidation of CO to CO_2, which may indicate that a CO adsorption step is the rds, consistent with the EIS data (Fig. 9,

Table 8). Even so, the performance of the LSFCr-3 electrode towards CO oxidation is quite good, comparable to other types of perovskites, such as LSCM [23].

It is also interesting that the CO_2 reduction currents are roughly 10 times higher in the CO_2/CO mixture used in Fig. 10 than in 100% CO_2, suggesting that the LSFCr-3 material is in a much different redox state in the two CO_2-containing environments. The potential of the CO_2/CO equilibrium is ca. 670 mV more negative (more reducing) than in pure CO_2, arguing that a higher concentration of Fe^{3+} should be present at the surface, leading to better catalytic activity. We expect Cr to remain in the +6 state under all conditions at the surface, in agreement with studies by Mizusaki [24] on $LaCrO_3$.

The excellent performance in the cathodic direction during CO_2 reduction could be due to preferential adsorption of CO_2 on the active sites and also an increase in oxygen vacancy concentration due to the reduction of Fe^{4+} to Fe^{3+}, which will favour the reduction of CO_2, according to reaction (1).

$$CO_2 + V_o^{\cdot\cdot} + 2e^- = O_o^x + CO \qquad (1)$$

This is in agreement with the explanation for R2 and C2 in Table 8, where a lower R2 and higher C2 is seen at -100 mV polarization vs. at the OCP.

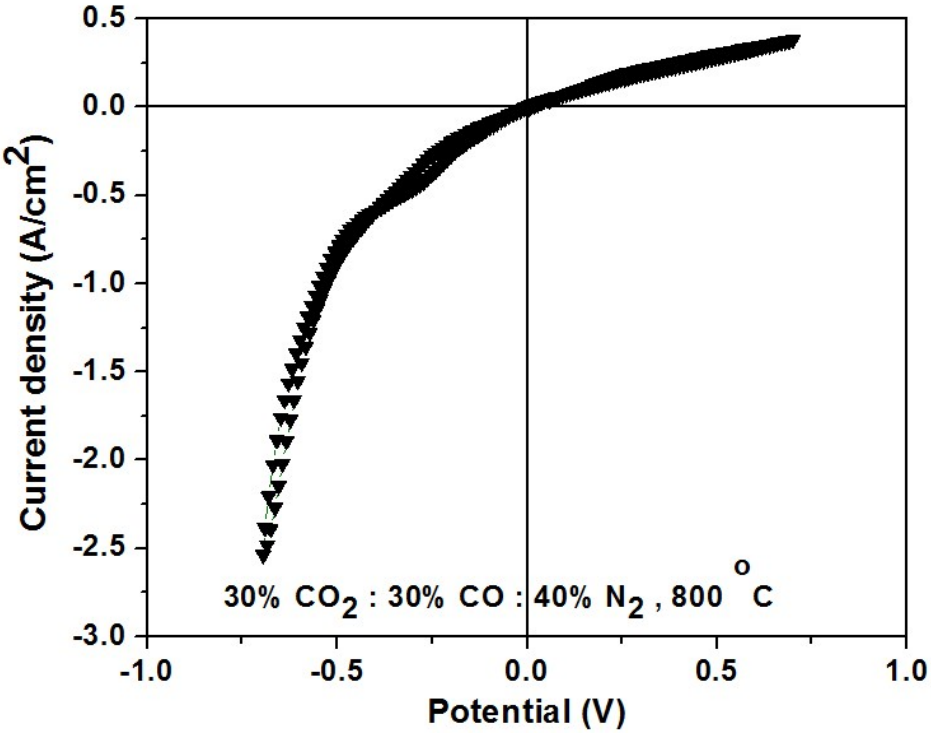

Fig. 10 Cyclic voltammetry data obtained for LSFCr-3 WE in 3 electrode half-cell at 800 ^{o}C in 30% CO_2:30%:40% N_2 at 1mV/ s.

To further analyze the CV data, the low field exchange current density (i_o) was obtained from the slope of the i-V plot (Fig 10) within ± 50 mV of the OCP, based on equation (3). For the CO_2/CO reduction reaction, n and ν were assumed to be 2 and 1, respectively (as the total number of electrons passed per molecule of CO_2 reduced is 2 and the number of occurrences of the rds (ν) would probably be 1). The i_o values obtained from this CV analysis were then compared to the i_o obtained from the the Rp of OCP EIS work (Table 8), giving similar values, i.e., 41 mA/cm^2 from the CV and 53 mA/cm^2 from the EIS data. These high current densities are fully consistent with the excellent activity of the LSFCr-3 catalyst towards the CO/CO_2 redox process. Notably, the high field Butler Volmer approximation was not used here, because it is questionable if Butler-Volmer formalisms can be applied to electrochemical data acquired at an

electrode material that is changing its composition (and catalytic activity) over the potential range being analyzed.

4. Conclusions

The electrochemical performance of LSFCr-3 has been studied in detail, both at open circuit and under polarization, in 3-electrode half-cells between 650 and 800 ^{o}C, in air, pure CO_2 and CO_2/CO mixtures. It is shown here, using impedance spectroscopy (EIS) and cyclic voltammetry (CV), that the performance of this material in all of these gas environments is very good. The 3 electrode half-cell configuration allowed us to isolate the reactions occurring in the fuel cell and electrolysis modes and determine the catalytic activity of the material towards each reaction separately. This showed that LSFCr-3 is a better catalyst for the oxygen evolution and CO_2 reduction reactions than for oxygen reduction or CO oxidation, indicating an overall better performance in the electrolysis vs. fuel cell mode.

Our results have also shown that the measured pO_2 dependence is very different at the OCP than under positive or negative polarization, while also revealing that the rate of oxygen evolution is independent of pO_2 under polarized conditions. No evidence for diffusion limitations (gas phase) were obtained from our EIS and CV experiments in air. In both air and CO/CO_2 environments, there is good evidence for the presence of a chemical capacitance, as also seen from the significant effect of the reducing atmosphere (CO_2 vs. CO_2/CO) on the rate of the CO/CO_2 redox reactions. This was ascribed to significant changes in the oxidation state of the Fe component in LSFCr-3 in these different gas environments.

Acknowledgements

We are grateful for the support of the NSERC Solid Oxide Fuel Cell Canada Strategic Research Network as well as Carbon Management Canada, a Canadian National Centre of Excellence. The authors gratefully acknowledge the Eyes High PDF Program at the University of Calgary and Alberta Innovates – Technology Futures (AITF) for the support of AB. We also would like to thank AITF for their scholarship support of PA.

References

1. M. Chen, S. Paulson, V. Thangadurai and V. Birss, *Journal of Power Sources*, 2013, **236**, 68-79.
2. B. Molero-Sánchez, J. Prado-Gonjal, D. Ávila-Brande, M. Chen, E. Morán and V. Birss, *International Journal of Hydrogen Energy*, 2015, **40**, 1902-1910.
3. J. C. Ruiz-Morales, D. Marrero-Lopez, J. Canales-Vazquez and J. T. S. Irvine, *RSC Advances*, 2011, **1**, 1403-1414.
4. S. Xu, S. Li, W. Yao, D. Dong and K. Xie, *Journal of Power Sources*, 2013, **230**, 115-121.
5. P. Addo, B. Molero-Sánchez, M. Chen, S. Paulson and V. Birss, 11th European SOFC and SOE forum, Luzerne, Switzerland, 2014.
6. D. Pérez-Coll, A. Aguadero, M. J. Escudero and L. Daza, *Journal of Power Sources*, 2009, **192**, 2-13.
7. Z. Lu, J. Hardy, J. Templeton and J. Stevenson, *Journal of Power Sources*, 2011, **196**, 39-45.
8. S. McIntosh, S. B. Adler, J. M. Vohs and R. J. Gorte, *Electrochemical and Solid-State Letters*, 2004, **7**, A111-A114.
9. R. Küngas, A. S. Yu, J. Levine, J. M. Vohs and R. J. Gorte, *Journal of The Electrochemical Society*, 2013, **160**, F205-F211.
10. M. J. Escudero, A. Aguadero, J. A. Alonso and L. Daza, *Journal of Electroanalytical Chemistry*, 2007, **611**, 107-116.
11. P. Hjalmarsson, M. Søgaard and M. Mogensen, *Solid State Ionics*, 2009, **180**, 1395-1405.
12. E. P. Murray, T. Tsai and S. A. Barnett, *Solid State Ionics*, 1998, **110**, 235-243.
13. S. P. Jiang, J. G. Love and Y. Ramprakash, *Journal of Power Sources*, 2002, **110**, 201-208.
14. D. Marinha, L. Dessemond and E. Djurado, *Journal of Power Sources*, 2012, **197**, 80-87.
15. F. S. Baumann, J. Fleig, H.-U. Habermeier and J. Maier, *Solid State Ionics*, 2006, **177**, 1071-1081.
16. F. S. Baumann, J. Maier and J. Fleig, *Solid State Ionics*, 2008, **179**, 1198-1204.

17. B. Liu, Y. Zhang and L. Zhang, *International Journal of Hydrogen Energy*, 2009, **34**, 1008-1014.
18. D. A. Noren and M. A. Hoffman, *Journal of Power Sources*, 2005, **152**, 175-181.
19. O'M. Bockris, *Modern Electrochemistry, vol. 2*, New York, NY 1973.
20. B. Molero-Sánchez, P. Addo, M. Chen, S. Paulson and V. Birss, 11 th European SOFC & SOE FORUM 2014, Luzern, Switzerland, 2014.
21. J. Liu, A. C. Co, S. Paulson and V. I. Birss, *Solid State Ionics*, 2006, **177**, 377-387.
22. F. M. Sapountzi, S. Brosda, K. M. Papazisi, S. P. Balomenou and D. Tsiplakides, *J Appl Electrochem*, 2012, **42**, 727-735.
23. X. Yue and J. T. S. Irvine, *Journal of The Electrochemical Society*, 2012, **159**, F442-F448.
24. J. Mizusaki, *Solid State Ionics*, 1992, **52**, 79-91.